The important role of rubidium hydroxide in the synthesis of hierarchical ZSM-5 zeolite using cetyltrimethylammonium as structure-directing agent

Document Version:
Publisher's PDF, also known as Version of Record (includes final page, issue and volume numbers)

Please check the document version of this publication:

• A submitted manuscript is the version of the article upon submission and before peer-review. There can be important differences between the submitted version and the official published version of record. People interested in the research are advised to contact the author for the final version of the publication, or visit the DOI to the publisher's website.
• The final author version and the galley proof are versions of the publication after peer review.
• The final published version features the final layout of the paper including the volume, issue and page numbers.

Link to publication

Zeolite Synthesis | *Very Important Paper* |

VIP

The Important Role of Rubidium Hydroxide in the Synthesis of Hierarchical ZSM-5 Zeolite Using Cetyltrimethylammonium as Structure-Directing Agent

Wannaruedee Wannapakdee,[a] Lingqian Meng,[b] Arno J. F. van Hoof,[b] Alexsei Bolshakov,[b] Chularat Wattanakit,[a] and Emiel J. M. Hensen*[b]

Abstract: Hierarchical ZSM-5 zeolite with uniform mesopores was synthesized with a simple cetyltrimethylammonium (CTA$^+$) template, which acted as a bifunctional surfactant in a RbOH-based alkaline synthesis gel. Rb$^+$ plays a key role in obtaining uniform mesopores within ZSM-5 crystals. The structural, textural properties and the acidity were characterized by XRD, Ar physisorption, TEM, as well as CO IR and ^{27}Al MAS NMR spectroscopy. These data point to partial retention of the initial meso-scale ordered texture of the precursor in the final zeolite. These textural properties result in a strongly improved catalytic performance in the methanol conversion reaction compared to bulk zeolite.

Introduction

Zeolites, which are microporous aluminosilicates, are widely used as catalysts in the petroleum refining and petrochemical industry.[1,2] Their crystalline framework displays unique properties such as high surface area, good chemical and thermal stability, strong Brønsted acidity and shape selectivity in catalytic transformation of hydrocarbons due to the specific arrangement of channels and cages.[3] On the other hand, the microporous nature of the pore system can result in slow diffusion of reactant and product molecules, which limits catalytic reactivity and may shorten catalyst lifetime due to increased coking rates.[4] In order to circumvent these problems, the introduction of a secondary system of larger pores in the zeolite framework can be considered. In practice, such hierarchical zeolites contain usually micropores and mesopores.[4] The additional porosity can be introduced by modifying existing zeolite crystals (e.g., dealumination or desilication) or by direct synthesis using hard or soft templates. Ryoo and co-workers[5,6] explored diquaternary ammonium surfactants (DQAS) as structure-directing agents (SDAs) for generating nanostructured ZSM-5 in a one-pot synthesis. The DQAS has two roles in this approach. Its hydrophilic part controls formation of zeolite structures by interaction of the head group with silica leading to pre-structured moieties that will later condense to zeolite MFI, while the hydrophobic hydrocarbon tail serves as a mesoporogen.[7] Despite the aesthetic beauty of these materials and their improved catalytic performance they remain mostly model catalysts, because typical DQAS are too expensive to synthesize nanostructured zeolites at an industrial scale.

In contrast to these DQAS, a single quaternary ammonium surfactant cetyltrimethylammonium (CTA$^+$) is a simple organic chemical. Interest in porous silicas based on CTA salts is rooted in the discovery of ordered mesoporous MCM-41, formed by condensation of silica on micellar rod arrays of the surfactant (e.g., CTA$^+$Br$^-$).[8,9] Beneficial properties of this class of mesoporous silicas are the high surface area, uniform pore size and high adsorption capacity.[10,11] But, they usually exhibit a low hydrothermal stability and display low catalytic performance, which is mainly due to the weak acidity of the protons arising from introduction of Al in the amorphous silica network.[12] Hence, many researchers have attempted to crystallize zeolites using CTA$^+$ with the idea to co-generate mesopores. Unfortunately, this nearly always results in microporous zeolites without additional mesoporosity.[13–16] Recently, our group presented a one-step method for synthesizing mesoporous ZSM-5 zeolites by a CTA$^+$ template using KOH as basic source.[17] The CTA$^+$ surfactant not only generates a secondary mesopore system, but is also involved as an SDA in the nucleation of MFI zeolite. It was found that replacing the usual NaOH base with KOH results in more facile dissolution of silica at elevated temperatures at which zeolite nucleation can occur. The resulting zeolites contain mesopores that are not uniform nor ordered, likely because KOH disturbs the formation of micellar rods of

[a] *Department of Chemical and Biomolecular Engineering, School of Energy Science and Engineering, Vidyasirimedhi Institute of Science and Technology,*
Rayong, 21210, Thailand
[b] *Inorganic Materials and Catalysis, Schuit Institute of Catalysis, Department of Chemical Engineering and Chemistry, Eindhoven University of Technology,*
P.O. Box 513, 5600 MB, Eindhoven, The Netherlands
E-mail: e.j.m.hensen@tue.nl
Supporting information and ORCID(s) from the author(s) for this article are available on the WWW under https://doi.org/10.1002/ejic.201900324.

ChemPubSoc
Europe

EurJIC
European Journal
of Inorganic Chemistry

Full Paper

CTA+ surfactants.[18,19] In this case, the morphology of the final small zeolite crystals is not related to that of the original mesoporous silica precursor.

The differences between NaOH and KOH mediated syntheses can be linked to the rate of silica dissolution, which depends on the radius of the hydrated cation that stabilized the negatively charged silica network at high pH.[20] The sodium cation is known as a water former because of its large hydrated shell of 0.36 nm.[21] In contrast, the larger potassium cation binds water molecules weaker, forming smaller and more diffuse hydration shells.[21] When these cations compensate the negative charge of amorphous silica precursors in zeolite synthesis gels, the more diffuse water shell for potassium allows for a more direct access to Si–O–Si bonds than the rigid shell around sodium. While potassium may give rise to a too high silica dissolution rate, thereby disrupting already formed micellar rod arrays in CTA-templated silica precursors,[19] the lower silica dissolution rate for rubidium with its slightly smaller hydration shell[18,19] might provide a way to preserve the initial order of the silica morphology during the transformation of amorphous silica to crystalline zeolite. Based on this, the goal of this work was to synthesize uniform mesoporous ZSM-5 zeolites using CTAOH as a bifunctional template in alkaline RbOH gels. The materials are extensively characterized for their physico-chemical and acidic properties. Their catalytic performance was evaluated in the methanol-to-hydrocarbon (MTH) reaction.

Results and Discussion

The synthesis procedures are described in detail in the SI. The crystal structure of the zeolites was determined by XRD. Figure S1 shows that the XRD patterns of MFI(C16TA, 7 d) before and after calcination are the same. XRD is also used to determine the ordering at different length scales of the calcined zeolites (Figure 1). The XRD patterns indicate that zeolite crystallization starts after 2 days and nearly fully crystalline zeolite is obtained after 4 days. Prolonged hydrothermal synthesis did not change the diffraction patterns. In the small-angle region (Figure 1), a pronounced feature at 1.94° is visible after 2 days, which grows and slightly shifts to higher angle during crystallization at 413 K. There is a weak shoulder at 2.96°. These peaks relate to the ordering of silica at the mesoscale, which is confirmed by the finding that the use of C20TA instead of C16TA results in a shift to lower angles (Figure 1) with a small loss of zeolite crystallinity as can be seen from Figure 1h. Notably, the XRD patterns of the C16TA- and C20TA-templated samples are different from the pattern typically observed for MCM-41 (Figure 1). The evolution of the patterns for MFI(C16TA) during hydrothermal synthesis implies that mesoscale order of silica was established before zeolite crystallization and also that this order was maintained during zeolite crystallization. Therefore, it is likely that the mesopores are integrated in the crystalline zeolite sample. We note however that there is less order than in a typical MCM-41 sample (Figure S2b).[22,23] We also found that a similar approach where RbOH was replaced by LiOH, NaOH or CsOH led to amorphous samples (Figure S3). Compared to our earlier work in which we used KOH to obtain hierarchical ZSM-5, the

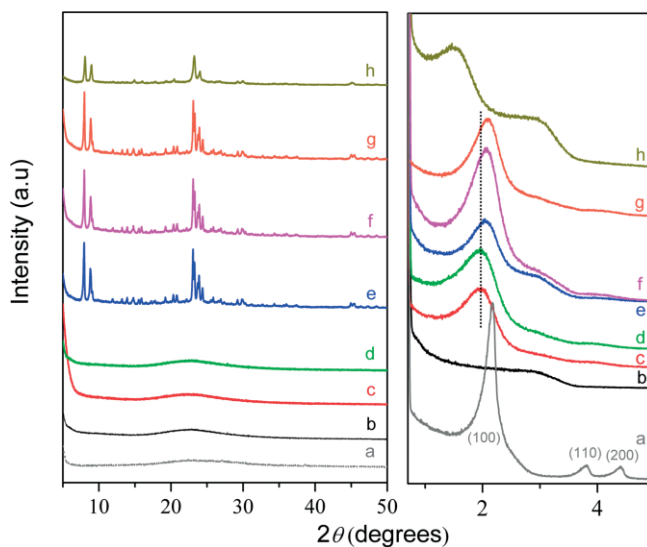mesopores in the RbOH-mediated synthesis are much more ordered.

Figure 1. XRD patterns of wide angle (left) and small angle (right) of calcined zeolites; (a) MCM-41 reference, (b) MFI(C16TA,0 d), (c) MFI(C16TA,1 d), (d) MFI(C16TA,2 d), (e) MFI(C16TA,4 d), (f) MFI(C16TA,5 d), (g) MFI(C16TA,7 d) and (h) MFI(C20TA,7 d).

Figure 2. shows Ar physisorption isotherms and pore size distributions (PSDs) for calcined zeolite samples as a function of the crystallization time. The corresponding textural properties are listed in Table S1. The isotherms for the samples obtained after 2, 5 and 7 days crystallization exhibit a typical type IV shape with a H2 hysteresis loop.[24,25] The steep Ar uptake at a low pressure ($P/P0 < 0.1$) is due to the filling of micropores, while the hysteresis loop at $P/P0 > 0.4$ points to the presence of mesopores. According to literature, the H2 hysteresis loop is characteristic for a narrow size distribution of mesopores.[25]

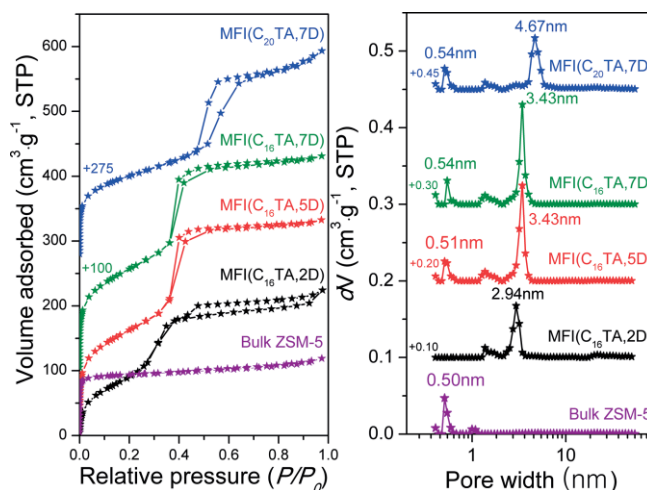Figure 2. Ar physisorption isotherms (left) and pore size distribution (right) of the calcined ZSM-5 zeolites using C16TAOH and C20TAOH surfactants. The pore size distributions were calculated by the NLDFT method using the adsorption branch.

The X-ray amorphous sample obtained after 2 days hydrothermal synthesis contained only mesopores with a narrow PSD around 2.94 nm (Figure 2). The absence of zeolitic micropores

ChemPubSoc
Europe

EurJIC
European Journal
of Inorganic Chemistry

Full Paper

in this material is consistent with the XRD patterns. In contrast, MFI(C$_{16}$TA, 5 d) and MFI(C$_{16}$TA, 7 d) obtained after longer crystallization contained micropores with a size characteristic for ZSM-5 zeolite. The amount of mesopores increased with crystallization time. The PSDs are centered around 3.43 nm. These changes go together with a strong increase of the BET surface area for the calcined materials, which is predominantly caused by the formation of micropores. Thus, the use of C$_{16}$TA in the RbOH-based alkaline synthesis mixture not only results in the formation of uniform mesopores, but also crystalline ZSM-5 zeolite. We found that the size of the alkyl chain of the SDA affects the mesopore size (Figure S2). Compared to the C$_{16}$TA-templated sample, the C$_{20}$TA-templated zeolite exhibited a broader peak at a higher diffraction angle (Figure 1), which can be explained by larger mesopores. This is in line with the larger on average 4.67 nm pores derived from Ar physisorption data (Figure 2). The textural properties of the various materials are more detailed in Table S1.

TEM images of materials obtained at various crystallization times are shown in Figure 3. The samples differ significantly in morphology. Briefly, the MFI(C$_{16}$TA,2 d) sample contains regions with uniform mesopores (Figure 3a). For the samples obtained after crystallization over 5 and 7 days, we observe that there are significant changes in the morphology. Clearly, rod-shaped zeolite crystals are formed, which are likely oriented along the earlier direction of the mesopore channels of the amorphous precursor materials. The crystalline rod-shaped domains are separated by mesopores. Inspection of larger areas of the sample crystallized for 7 days shows that most of the amorphous mesostructured precursor phase has been transformed into crystalline zeolite. This conversion is in line with the high micropore volume of 0.12 cm^3 g^{-1} (NLDFT), comparable to the value recorded for bulk ZSM-5 zeolite, and the absence of a broad feature in the XRD pattern characteristic for amorphous silica. Thus, although the precursor morphology is not fully retained, the final crystalline mesoporous zeolite contains some of the features of the precursor, as evident from the textural analysis and TEM.

Based on these observations, we propose a mechanism of the formation of mesoporous ZSM-5 zeolites (Scheme 1). Initially, an amorphous silica-surfactant assembly is formed at low temperature, which contains some ordered mesoporosity that resembles that in MCM-41. The lower mesoscale order relates to the use of RbOH as a base. When the mixture is brought to hydrothermal conditions, zeolite crystallization occurs after a few days. In a comparable synthesis with NaOH, the amorphous precursor is not dissolved, while with KOH most of the precursor dissolves, resulting in a mesoporous zeolite with another morphology than obtained with RbOH. The RbOH case is intermediate in the sense that the texture and morphology retains some of the features of the ordered mesoporous structure of the amorphous precursor. The widening of the mesopores shows the transformation from amorphous silica to crystalline zeolite involves some silica dissolution, implying that this synthesis does not represent a case of a solid–solid transformation. This is understandable as the zeolite crystal domains observed by TEM are larger than the thin silica walls of the amorphous precursor. We also verified that in a synthesis without CTAOH only amorphous silica was obtained (Figure S4).

We then investigated the acid strength of the calcined and ammonium-exchanged MFI(C$_{16}$TA,7 d) and bulk ZSM-5 catalysts. CO IR spectra measured at liquid nitrogen temperature are shown in Figure 4a. The equal red shift of 316 cm^{-1} of the bridging hydroxyl groups evidences that both samples contain similar strong Brønsted acid sites. Also the intensities of the relevant bridging hydroxyl groups are similar for both samples. ^{27}Al MAS NMR of the calcined samples confirms that most Al atoms are present in the zeolite framework (Figure 4b).

To illustrate the beneficial effect of the mesopores in the ZSM-5 crystals, we compared the catalytic performance of the mesoporous zeolites in the MTH reaction to a bulk ZSM-5 sample. Besides its practical relevance, this reaction also serves as a model reaction for evaluating the influence of increased accessibility of the zeolite domains. In the MTH reaction, methanol is converted to light olefins, mostly C$_3$ and higher olefins, as well as higher hydrocarbons. Competing is the formation of coke deposits that block the zeolite micropores and deactivates the catalyst. This type of coking deactivation is fast for bulk ZSM-5 zeolite, where methanol diffusion is slow compared to the reaction rate. At typical conditions (WHSV = 6 h^{-1}; T = 673 K), the initially complete conversion of bulk ZSM-5 zeolite decreases to 50 % in about 7 h (Figure 4c). The mesoporous zeolites deactivate much slower: the time for MFI(C$_{16}$TA,7 d) to reach 50 % conversion is 36 h. Notably, the mesoporous zeolites display a slightly higher light olefins selectivity and lower aromatics selectivity than bulk ZSM-5 (Table S2), which is likely due to the reduced average residence time in the mesoporous zeolite.
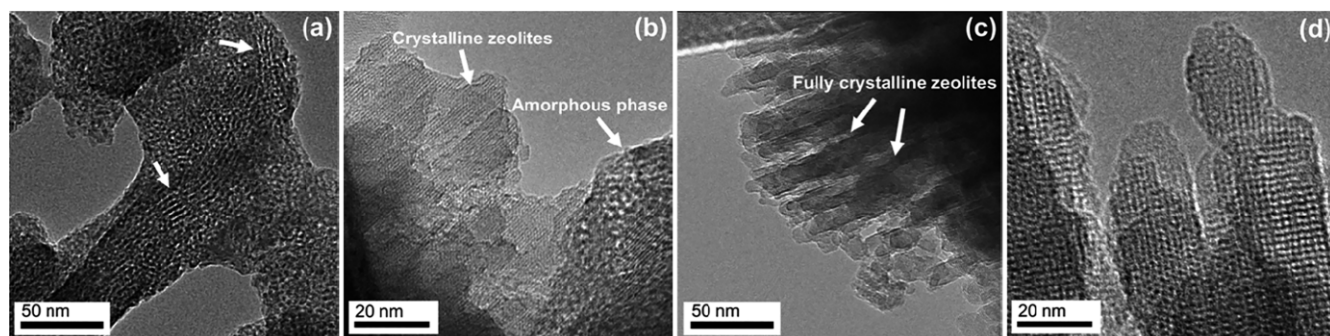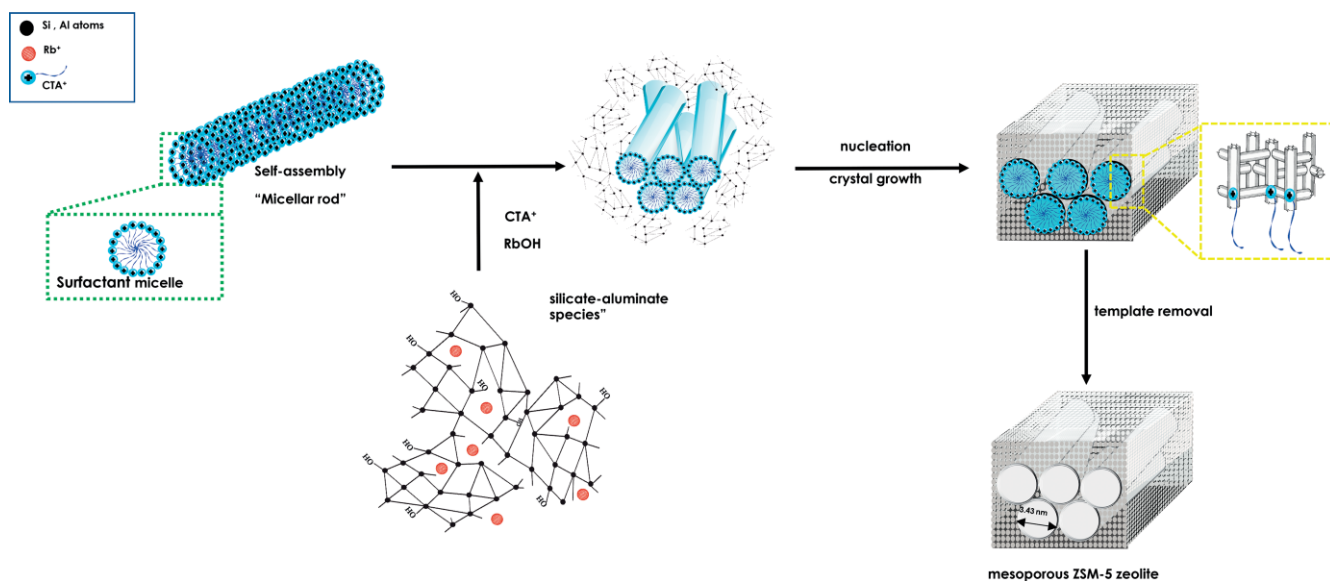

Figure 3. TEM images of (a) MFI(C$_{16}$TA,2 d), (b) MFI(C$_{16}$TA,5 d), (c) MFI(C$_{16}$TA,7 d) and (d) HRTEM of MFI(C$_{16}$TA,7 d) samples.

★ ChemPubSoc
Europe

EurJIC
European Journal
of Inorganic Chemistry

Full Paper

Scheme 1. Proposed mechanism of the formation of mesoporous ZSM-5 zeolites: The amphiphilic surfactant self-assembles into micellar rods, with the length of the hydrophobic tail of the surfactant determining the diameter of the micelles. Simultaneously, amorphous silica-alumina species aggregate around these micelles by electrostatic interactions. During hydrothermal synthesis, the ammonium head group of CTA^+ induces ZSM-5 crystal growth through interactions with this amorphous silica-alumina phase, under retention of the mesoscale structure. A crucial role is played by Rb_+, which compensates the charge of the negatively charged surface of the amorphous silica-alumina precursor. Compensation by Rb_+ instead of Na_+ allows for dissolution of sufficient silicate species to start zeolite nucleation close to the surface of the meso-structured silica-alumina precursor, leading to a final zeolite morphology akin to the mesostructured precursor. After removal of the organic template by calcination in air, uniform mesopores remain between the obtained ZSM-5 zeolite crystals.Proposed mechanism of the formation of mesoporous ZSM-5 zeolites.
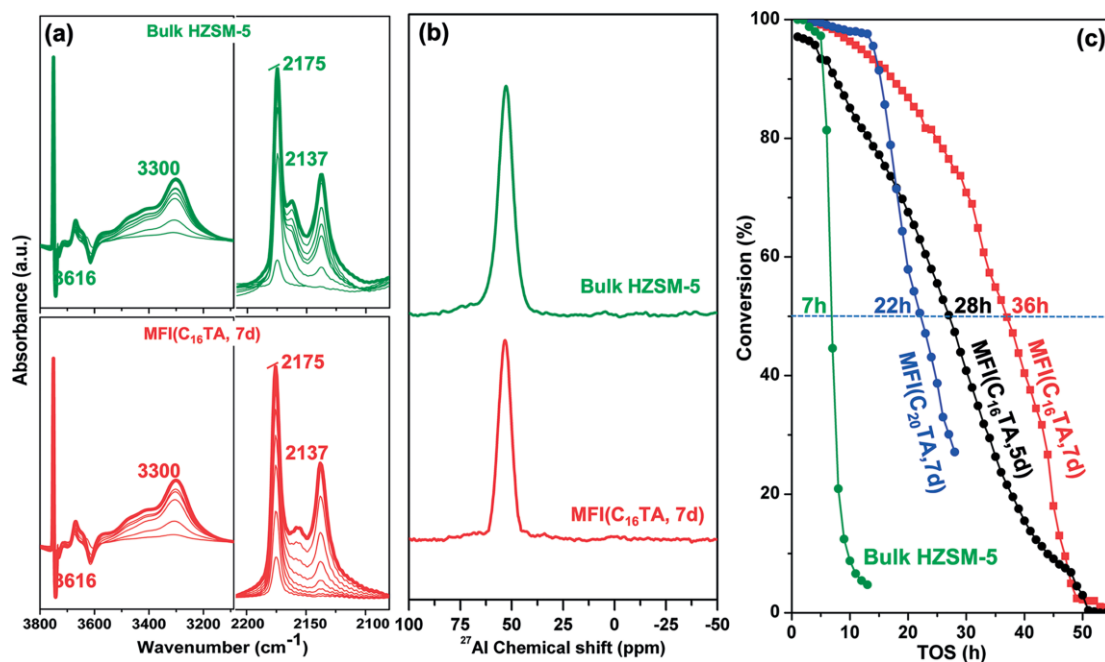

Figure 4. (a) OH (3800 cm^{-1} – 3000 cm^{-1}) and CO stretching regions (2280 cm^{-1} – 2050 cm^{-1}) of IR spectra of bulk ZSM-5 (green) and mesoporous MFI(C_{16}TA,7 d) (red) zeolites recorded at 77 K. The bolder spectra represent the spectra at the highest CO coverage. (b) ^{27}Al MAS NMR spectra. (c) Methanol conversion of bulk and mesoporous ZSM-5 zeolites as a function of time-on-stream. The lifetime as defined by the time to reach a methanol conversion of 50 % is indicated.

Conclusions

We achieved the synthesis of hierarchical ZSM-5 zeolite with uniformly sized mesopores well integrated into the crystalline zeolite phase. Essential to this unusual synthesis is the combination of RbOH as a base with an amphiphilic surfactant that pre-

orders the amorphous silica into a mesophase. The use of Rb cations modifies the silica dissolution rate in such way that the mesoporous texture of the amorphous precursor is retained to some extent. The resulting mesoporous zeolite contains acid sites similar in density and strength as a bulk ZSM-5 reference zeolite. As a result of the high interconnectivity of the micro-

pores and mesopores, the catalytic performance in the MTH reaction of ZSM-5 is strongly enhanced after the introduction of mesopores. This work shows that judicious choice of the basic cation in zeolite synthesis gels can aid in controlling the mesoscale morphology.

Acknowledgments

[1] A. Hagen, F. Roessner, *Catal. Rev.* **2000**, *42*, 403–437.
[2] C. R. Bayense, J. H. C. van Hooff, *Appl. Catal. A* **1991**, *79*, 127–140.
[3] K. Möller, T. Bein, *Chem. Soc. Rev.* **2013**, *42*, 3689–3707.
[4] G. Kocasoy, V. Şahin, *J. Environ. Sci. Health Part A* **2007**, *42*, 2139–2146.
[5] M. Choi, R. Srivastava, R. Ryoo, *Chem. Commun.* **2006**, *0*, 4380–4382.
[6] M. Choi, K. Na, J. Kim, Y. Sakamoto, O. Terasaki, R. Ryoo, *Nature* **2009**, *461*, 246–249.
[7] X. Zhang, D. Liu, D. Xu, S. Asahina, K. A. Cychosz, K. V. Agrawal, Y. Al Wahedi, A. Bhan, S. Al Hashimi, O. Terasaki, M. Thommes, M. Tsapatsis, *Science* **2012**, *336*, 1684–1687.
[8] M. Ebrahimi-Gatkash, H. Younesi, A. Shahbazi, A. Heidari, *Appl. Water Sci.* **2017**, *7*, 1887–1901.
[9] Y. Ma, H. Chen, Y. Shi, S. Yuan, *Mater. Res. Bull.* **2016**, *77*, 258–264.
[10] J. S. Beck, J. C. Vartuli, W. J. Roth, M. E. Leonowicz, C. T. Kresge, K. D. Schmitt, C. T. W. Chu, D. H. Olson, E. W. Sheppard, S. B. McCullen, J. B. Higgins, J. L. Schlenker, *J. Am. Chem. Soc.* **1992**, *114*, 10834–10843.
[11] E. Dündar-Tekkaya, Y. Yürüm, *Int. J. Hydrogen Energy* **2016**, *41*, 9789–9795.
[12] Y. Fang, H. Hu, *J. Am. Chem. Soc.* **2006**, *128*, 10636–10637.
[13] T. Moteki, S. H. Keoh, T. Okubo, *Chem. Commun.* **2014**, *50*, 1330–1333.
[14] T. Moteki, S. H. Keoh, T. Ohmura, K. Iyoki, T. Wakihara, T. Okubo, *J. Ceram. Soc. JPN.* **2013**, *121*, 575–577.
[15] X. Wang, H. Chen, F. Meng, F. Gao, C. Sun, L. Sun, S. Wang, L. Wang, Y. Wang, *Microporous Mesoporous Mater.* **2017**, *243*, 271–280.
[16] L. Xu, X. Ji, S. Li, Z. Zhou, X. Du, J. Sun, F. Deng, S. Che, P. Wu, *Chem. Mater.* **2016**, *28*, 4512–4521.
[17] L. Meng, B. Mezari, M. G. Goesten, E. J. M. Hensen, *Chem. Mater.* **2017**, *29*, 4091–4096.
[18] P. W. J. G. Wijnen, T. P. M. Beelen, K. P. J. Rummens, R. A. van Santen, *J. Non-Cryst. Solids* **1993**, *152*, 127–136.
[19] P. W. J. G. Wijnen, T. P. M. Beelen, J. W. de Haan, C. P. J. Rummens, L. J. M. van de Ven, R. A. van Santen, *J. Non-Cryst. Solids* **1989**, *109*, 85–94.
[20] M. T. Tognonvi, J. Soro, S. Rossignol, *J. Non-Cryst. Solids* **2012**, *358*, 81–87.
[21] K. Shomglin, L. Turanli, H. R. Wenk, P. J. M. Monteiro, G. Sposito, *Cem. Concr. Res.* **2003**, *33*, 1825–1830.
[22] A. J. Schwanke, C. W. Lopes, S. B. C. Pergher, *Mater. Sci. Appl.* **2013**, *4*, 68–72.
[23] C.-Y. Chen, S.-Q. Xiao, M. E. Davis, *Micropor. Mater.* **1995**, *4*, 1–20.
[24] S. W. S. Kenneth, T. W. Ruth, *Adsorpt. Sci. Technol.* **2004**, *22*, 773–782.
[25] M. Thommes, *Chem. Eng. Technol.* **2010**, *82*, 1059–1073.